Towards 3D passive shear elasticity imaging using row-columns arrays

Miguel Bernal[*], Nicolás Benech[+], Ron Daigle[*], Javier Brum[+]
[*]Verasonics Inc., Kirkland WA, USA
[+]Laboratorio de Acústica Ultrasonora, Instituto de Física, Facultad de Ciencias, Universidad de la República, Montevideo, Uruguay
Emails: miguelbernal@verasonics.com, jbrum@fisica.edu.uy

***Abstract*— The stiffening of soft tissues has been demonstrated to be associated with different disease processes such as cancer. In the last decades several devices and techniques have been developed to provide 2D maps of elasticity in order to help in diagnosis. 3D shear elasticity imaging was recently implemented with matrix arrays using the acoustic radiation force of ultrasound as shear wave source. However, matrix arrays require large number of channels and data to be processed. Row Column Arrays (RCAs) are a cheaper alternative to volume imaging since they require lower number of channels. However, at present RCAs are unable to generate acoustic radiation force due to their design and manufacturing process. To overcome the need of acoustic radiation force for elasticity imaging, in this work we implemented a passive elastography approach based on noise correlation of a complex elastic wave field to conduct 3D shear elasticity imaging using RCAs. Experiments were conducted on a tissue mimicking phantom demonstrate the feasibility of this approach.**

Keywords*— row column array, ultrasound, elastography, noise-correlation, time reversal, volume imaging

I. Introduction

The elasticity of soft tissues has been demonstrated to correlated with their state of health. Some pathological processes such as cancer and liver fibrosis are known to cause stiffening of the tissues. Therefore, the ability of map the elasticity has diagnostic value and provides information that cannot be obtained by other means. Nowadays, devices that map elasticity in 2D are commonplace. However, the diagnostic value of these images can be greatly enhanced if the information is provided in 3D.

Three-dimensional ultrafast ultrasonic imaging is now possible thanks to the development of breakthrough technology like matrix [1] and row columns arrays (RCAs) [2],[3]. Moreover, Shear Wave Elastography relies on ultrafast acquisition to track the propagation of shear wave in the soft tissues. By determining its speed of propagation it is possible to image tissue's shear elasticity (μ), since $\mu = \rho c_s^2$, where ρ and c_s correspond to the tissue's density and shear wave velocity, respectively. Most available SWE commercial systems use the acoustic radiation force of a focused ultrasound beam to generate shear waves and locally estimate c_s to provide 2D shear elasticity images [4].

Recently, 3D shear elasticity imaging was implemented with matrix arrays using the acoustic radiation force of ultrasound as shear wave source [1],[5]. The main drawback of matrix arrays is that they require an ultrasound system with a large number of channels making this an expensive implementation. Contrary, RCAs allow volume imaging with lower channel count and have been used for 3D ultrafast acquisitions [6]. However, despite the advancement in probe manufacture, currently RCAs are unable to generate shear waves levels of acoustic radiation force. To overcome this limitation, in this work we implemented a passive elastography approach based on noise correlation of a complex elastic wave field to conduct 3D shear elasticity imaging using RCAs.

II. Materials and Methods

A. Experimental setup

Experiments were conducted on a bilayer tissue mimicking phantom made of gelatin. The top and bottom layers of the phantom were created with 4% and 7% gelatin by volume, respectively. Cornstarch was added to the gelatin solution to create ultrasonic speckle. The diameter of the phantom was 12 cm, and the top and bottom layers had a thickness of 4 cm and 10 cm, respectively (Fig. 1). Prior to the RCA experimentation, the shear wave velocity of each layer was measured using a SWE sequence as in [7] implemented on a Vantage 256 system with an L7-4 linear array. Shear wave velocities of 2.7 m/s and 4.8 m/s were found for the top and bottom layer, respectively.

In the 3D elasticity imaging experiments, a complex elastic wave-field dominated by shear waves was created inside the phantom by randomly taping the phantom's accessible surface with fingers following a similar procedure to [8],[9]. The tapping of the phantom was started two seconds prior to launching the ultrasound sequence and kept throughout the entire acquisition.

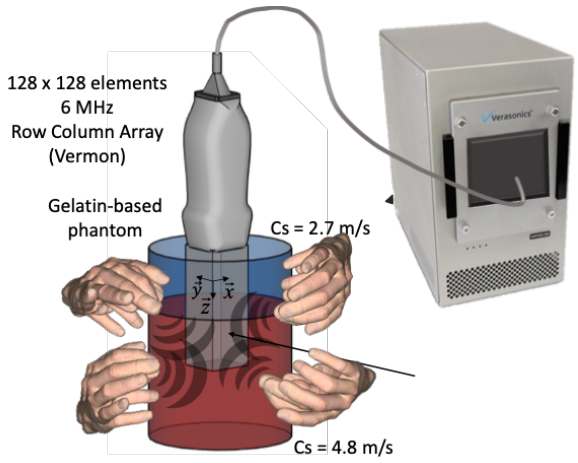

Fig. 1 Schematic representation of the experimental setup. Multiple finger impacts are used to create a complex elastic field within a bilayer tissue mimicking phantom. The particle velocity field is the acquired inside an imaging volume using a RCA driven by a Verasonics Vantage system.

B. *Ultrasonic sequence*

The z-component of the 3D particle velocity field (V_p) associated with the complex wavefield was acquired with plane wave insonifications using a Vantage 256 system and a 6 MHz RCA (Vermon SA). The probe has 256 elements (128 rows and 128 columns) and an acoustic footprint of 25.6 x 25.6 mm. The ultrasound acquisition lasted 2 seconds at a frame rate of 200 Hz for a total of 400 frames. For computing V_p (x,y,z,t), cross-correlation on the phase of the IQ-data of consecutive frames was used. The particle velocity field along the x and y directions were computed independently and averaged for the final result shown in Fig. 2.

C. *Cross-correlation and time reversal of shear waves: the derivative ratio method*

To recover a local shear wave velocity estimation, a cross-correlation approach interpreted as time reversal (TR) experiment was used in this work. Cross-correlation methods allow to reconstruct a refocusing wavefield from an apparently random and disorganized wavefield [10]. Let $\varphi(\mathbf{r},t)$ denote any quantity obeying a lossless wave equation, for example, the particle velocity field V_p measured in this work.

Then, the cross-correlation field (C) between signals acquired at different positions $\mathbf{r}$ and $\mathbf{r_o}$ can be computed as:

$$C(\mathbf{r},\mathbf{r_o},t) = \varphi(\mathbf{r},t) * \varphi(\mathbf{r_o},-t) \approx \varphi^{TR}(\mathbf{r},t) \qquad (1)$$

Where * denotes the convolution in time. Under the assumption of the field being diffuse, the time derivative of the cross-correlation in (1) is directly linked to the reversal field [10],[11]. Moreover, if the field φ has a finite bandwidth (as in most experiments), the correlation and its time derivative only differ in a constant phase factor [12] and the correlation field may be directly interpreted as the time reversal field. Thus, (1) represents a refocusing process around $\mathbf{r_o}$ with the focusing time set as 0 ms.

From the computed correlation field there are different independent approaches to image the shear wave velocity, for example, tracking the coherent shear wave as it focuses. Another alternative is to measure the focus size which is directly linked to the shear wavelength (λ_s) and hence to the shear wave velocity. Other authors have used the vibration amplitude at the focusing point, since for a given frequency, the vibration amplitude is larger in a soft tissue than in a hard one. A summary of these and other methods is given in [11]. In the current work we used the "derivative ratio" method which has been demonstrated to be less sensitive to the diffusivity hypothesis and has shown to be compatible with low imaging frame rates [11],[13].

D. *The derivative ratio method*

The derivative ratio method was first proposed by Catheline and his group in 2013 [13] and it was further refined by Zemzemi *et al.* who incorporated near field effects to the inversion [14]. The idea behind this method is the following: let $\varphi(\mathbf{r},t)$ represents a physical magnitude obeying a wave equation, then, its temporal ($\upsilon = \partial\varphi/\partial t$) and spatial derivatives ($\varepsilon_i = \partial\varphi/\partial i$, i = x,y,z) will obey a wave equation as well. Therefore, they are time reversal invariants. Under plane wave decomposition the time reversal version of each quantity (denoted with superscripts TR) can be written as [13]

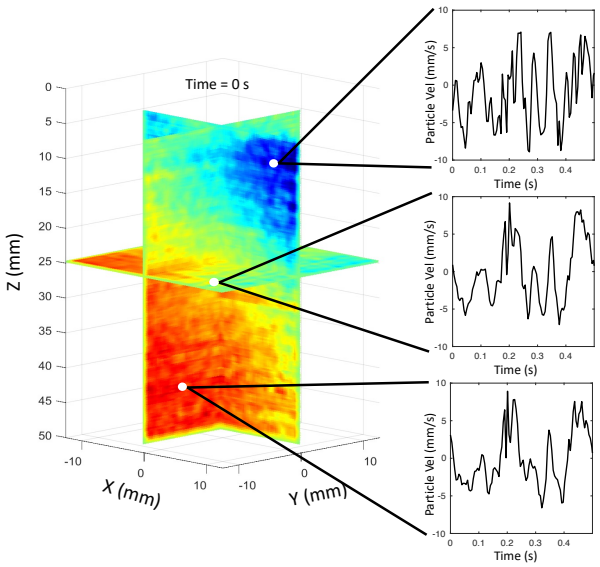

Fig. 2 Volumetric particle velocity field V_p used for shear wave velocity estimation. The left panel shows three different planes corresponding to x = 0 mm, y = 0 mm and z = 25 mm acquired at t = 0 s. The right panel shows a 0.5 s time window of the temporal trace of V_p for different points within the imaging volume. Each point is highlighted by white dots on the left panel.

$$\varepsilon_i^{TR}(\mathbf{r},\mathbf{r_o},t) = -k_i^2\,\varphi^{TR}(\mathbf{r},t) \qquad (2)$$

$$\upsilon^{TR}(\mathbf{r},\mathbf{r_o},t) = -\omega^2\,\varphi^{TR}(\mathbf{r},t) \qquad (3)$$

Where k_i is the i-component of the wave number and ω is the frequency. Consequently, the shear wave speed can be computed as the ratio between the time reversal version of the temporal and spatial derivatives at the focusing point. Moreover, to take advantage of the 3D information, in this work the shear wave velocity at point $\mathbf{r_o}$ was computed as:

$$c_s(\mathbf{r_o}) = \omega/k = \sqrt{\frac{\upsilon^{TR}(\mathbf{r_o},\mathbf{r_o},t=0)}{\sum_{i=x,y,z}\varepsilon_i^{TR}(\mathbf{r_o},\mathbf{r_o},t=0)}} \qquad (4)$$

Given the fact that time reversal focusing is a matched filter, another advantage of this approach is that it uses the maximum achievable signal to noise ratio for position $\mathbf{r_o}$.

So for the inversion (i.e. measuring $c_s(\mathbf{r_o})$) we let $\varphi(\mathbf{r},t)$ be V_p $(\mathbf{r},t)$. Therefore, we first compute the 3D gradient and temporal derivatives. Then, we computed the autocorrelation given in (1) at position $\mathbf{r_o}$ for each of the derivatives. This corresponds to the time reversal version of each quantity as expressed in (2) and (3). Finally, we applied (4) to recover c_s.

III. RESULTS AND DISCUSSION

Figure 3 shows the volumetric B-mode image of the phantom, where the boundary between both layers is visible for z ~ 28 mm.

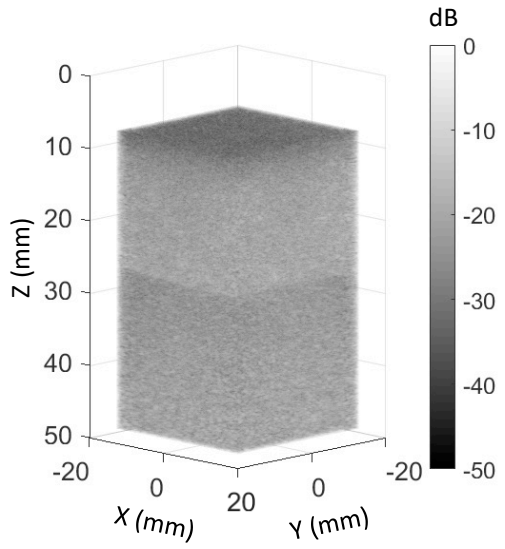

Fig. 3 Three-dimensional B-mode image of the two layered phantom. The interface between both layers is visible around z~28 mm.

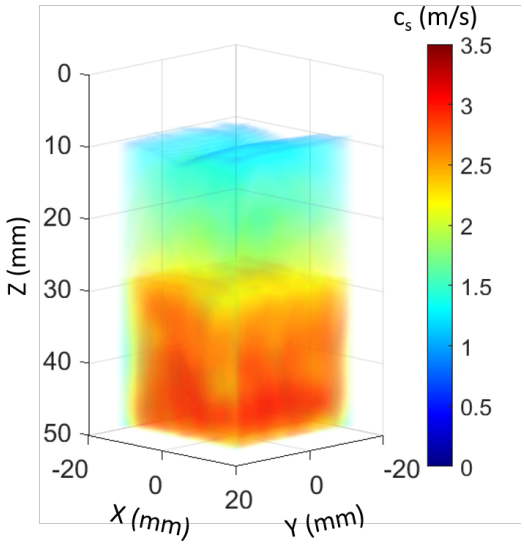

Fig. 4 Three dimensional shear wave velocity image. Both layers are clearly visible with mean shear wave velocities of 1.5 m/s and 2.6 m/s for the top and bottom layer respectively.

The 3D shear wave velocity image obtained using the passive elastography approach introduced in this work is shown in Fig. 4. In the volumetric shear wave velocity image both layers are clearly visible. The location of the sharp boundary between both layers is observable at z ~ 30 mm in fair agreement with the B-mode image, illustrating the spatial resolution of the method [14].

The values of c_s for the top and bottom layer were found to be 1.5 ± 0.003 m/s and 2.6 ± 0.008 m/s (mean value ± standard deviation), respectively. These values are lower than the ones measured during the elastic characterization of the phantom with values of 2.7 m/s and 4.8 m/s, respectively. This underestimation may be attributed to guidance effects, since the central frequency of the wave field was ~20 Hz (Fig. 2), thus resulting in shear wavelengths comparable to the thickness of each layer, i.e. λ_s ~ 13 cm and 24 cm for thicknesses of 4 cm and 10 cm, respectively. However, despite this underestimation a shear wave velocity contrast of 0.58 is found between both layers in good agreement with 0.56 found for our previous characterization.

In this work a complex wave field was generated using finger impacts over the phantom's accessible surface. The amplitude of the particle velocity field (~ 8 mm/s in Fig. 2) is larger than those in radiation-force methods Thus, the wave field was easily detected with the RCA.

The main drawback of this approach is that due to limited acquisition time and available surface for tapping the generated wave filed was not completely diffuse. Although diffusivity is strictly not needed for the derivative ratio method, this condition may enhance the final elasticity image [11],[13]. Despite these constraints, the passive elastography methods proposed in this work (Fig. 4) showed show a good agreement in differentiating the two layers with the B-mode image (Fig. 3). Future studies should focus on quantifying the impact of diffusivity in the final shear elasticity image and the use of more complex phantoms.

IV. CONCLUSIONS

The result of this proof of concept demonstrates the potential of RCAs combined with a passive elastography approach for 3D shear wave velocity imaging. Future works should focus on explaining the observed underestimation and imaging smaller inclusions.

ACKNOWLEDGMENT

N. B. and J. B. thank the support of PEDECIBA-Física, Uruguay, Comisión Sectorial de Investigación Científica (CSIC)-Uruguay and the Agencia Nacional de Investigación e Innovación (ANII) – Uruguay.

REFERENCES

[1] J. Provost, C. Papadacci, J. E. Arango, M. Imbault, M. Fink, J. L. Gennisson, M. Tanter, M. Pernot, "3D ultrafast ultrasound imaging in vivo," in Phys. Med. Biol, vol. 59, nr. 19, p. L1, September 2014.

[2] M. F. Rasmussen, T. L. Christiansen, E. V. Thomsen and J. A. Jensen, "3-D imaging using row-column-addressed arrays with integrated apodization - part i: apodization design and line element beamforming," in IEEE Transactions on Ultrasonics, Ferroelectrics, and Frequency Control, vol. 62, no. 5, pp. 947-958, May 2015.

[3] T. L. Christiansen, M. F. Rasmussen, J. P. Bagge, L. N. Moesner, J. A. Jensen and E. V. Thomsen, "3-D imaging using row–column-addressed arrays with integrated apodization— part ii: transducer fabrication and experimental results," in IEEE Transactions on Ultrasonics, Ferroelectrics, and Frequency Control, vol. 62, no. 5, pp. 959-971, May 2015.

[4] R. Sigrist, J. Liau, A. E. Kaffas, M. C. Chammas, J. K. Willmann, "Ultrasound Elastography: Review of Techniques and Clinical Applications," Theranostics, vol. 7, nr. 5, pp. 1303–1329, 2017.

[5] J. L. Gennisson, J. Provost, T. Deffieux, C. Papadacci, M. Imbault, M. Pernot, M. Tanter, "4-D ultrafast shear-wave imaging." IEEE Trans. Ultrason. Ferrelectr. Freq. Control, vol. 62, nr. 6, pp. 1059-1065, June 2015.

[6] A. Bertolo, J. Sauvage, M. Tanter, M. Pernot and T. Deffieux, "XDoppler: cross-correlation of orthogonal apertures for 3D blood flow imaging," in IEEE Trans. Med. Imag., doi: 10.1109/TMI.2021.3084865, 2020.

[7] M. Bernal, J. Saldarriaga, C. Cabeza, C. Negreira, J. Bustamante, J. Brum, "Development and evaluation of anisotropic and nonlinear

aortic models made from clinical images for in vitro experimentation," Phys. Med. Biol., vol. 64, nr. 16, 165006, 2019.

[8] T. Gallot, S. Catheline, P. Roux, J. Brum, N. Benech, C. Negreira, "Passive elastography: shear-wave tomography from physiological-noise correlation in soft tissues," in IEEE Trans. Ultrason. Ferroelectr. Freq. Control, vol. 58, pp.1122–6, 2011.

[9] J. Brum, S. Catheline, N. Benech, C. Negreira, "Quantitative shear elasticity imaging from a complex elastic wavefield in soft solids with application to passive elastography," in IEEE Trans. Ultrason. Ferroelectr. Freq. Control, vol. 62, pp. 673–85, 2015.

[10] F. J. Sánchez-Sesma, J. A. Pérez-Ruiz, F. Luzón, M. Campillo, A. Rodríguez-Castellanos, "Diffuse fields in dynamic elasticity," in Wave Motion, vol. 45, pp. 641–654, 2008.

[11] J. Brum, N. Benech, T. Gallot, C. Negreira, "Shear Wave Elastography Based on Noise Correlation and Time Reversal," in Front. Phys., vol. 9, 617445, 2021.

[12] P. Roux, K. G. Sabra, W. A. Kuperman, A. Roux, "Ambient noise cross correlation in free space: theoretical approach," in J. Acoust. Soc. Am., vol. 117, pp. 79–84, 2005.

[13] S. Catheline, R. Souchon, M. Rupin, J. Brum, A. H. Dinh, J.-Y. Chapelon, "Tomography from diffuse waves: passive shear wave imaging using low frame rate scanners," Appl. Phys. Lett., 103:014101, 2013.

[14] C. Zemzemi, A. Zorgani, L. Daunizeau, S. Belabhar, R. Souchon, S. Catheline, "Super-resolution limit of shear-wave elastography," European Phys. Lett., 129:34002, 2020.